J. Fluid Mech. (1991), *vol.* 227, *pp.* 35–46
Printed in Great Britain

Chaos in small-amplitude surface gravity waves over slowly varying bathymetry

By MICHAEL G. BROWN, FREDERICK D. TAPPERT AND SEKHAR E. R. B. SUNDARAM

Rosenstiel School of Marine and Atmospheric Science, University of Miami, 4600 Rickenbacker Causeway, Miami, FL 33149, USA

(Received 6 August 1990 and in revised form 14 November 1990)

We consider the motion of small-amplitude surface gravity waves over variable bathymetry. Although the governing equations of motion are linear, for general bathymetric variations they are non-separable and cannot be solved exactly. For slowly varying bathymetry, however, approximate solutions based on geometric (ray) techniques may be used. The ray equations are a set of coupled nonlinear ordinary differential equations with Hamiltonian form. It is argued that for general bathymetric variations, solutions to these equations – ray trajectories – should exhibit chaotic motion, i.e. extreme sensitivity to initial and environmental conditions. These ideas are illustrated using a simple model of bottom bathymetry, $h(x, y) = h_0(1 + \epsilon \cos(2\pi x/L) \cos(2\pi y/L))$. The expectation of chaotic ray trajectories is confirmed via the construction of Poincaré sections and the calculation of Lyapunov exponents. The complexity of chaotic geometric wavefields is illustrated by considering the temporal evolution of (mostly) chaotic wavecrests. Some practical implications of chaotic ray trajectories are discussed.

1. Introduction

In this paper we consider the motion of small-amplitude surface gravity waves over variable bathymetry. Although the governing equations of motion for the surface displacement $\zeta(x, y, t)$ are linear, they can be solved analytically only for very special bathymetric variations which allow variables to be separated. for general (non-separable) bathymetry which varies slowly on a scale of wavelengths, a geometric approximation is often made to simplify the problem. We assume that the bathymetric variations are sufficiently gradual that the geometric approximation is valid, and examine the behaviour of surface gravity waves in this limit.

It is well known (see e.g. Landau & Lifshitz 1959; or Whitham 1974) that the ray equations describing small-amplitude surface gravity waves are a system of coupled nonlinear ordinary differential equations,

$$\frac{\mathrm{d}x}{\mathrm{d}t} = \frac{\partial \omega}{\partial k_x}, \quad \frac{\mathrm{d}k_x}{\mathrm{d}t} = -\frac{\partial \omega}{\partial x}, \qquad \frac{\mathrm{d}y}{\mathrm{d}t} = \frac{\partial \omega}{\partial k_y}, \quad \frac{\mathrm{d}k_y}{\mathrm{d}t} = -\frac{\partial \omega}{\partial y}, \tag{1a–d}$$

where

$$\omega^2 = gk \tanh kh. \tag{2}$$

Here $\boldsymbol{k} = (k_x, k_y)$ is the wavenumber vector, $k = |\boldsymbol{k}| = (k_x^2 + k_y^2)^{\frac{1}{2}}$, g is the gravitational acceleration, ω is the frequency, and $h = h(x, y)$ is the water depth. Equations (1) define an autonomous Hamiltonian system with two degrees of freedom. The frequency

$$\omega = \omega(x, y, k_x, k_y), \tag{3}$$

which is a function of the generalized coordinates, x and y, and the corresponding momentum variables, k_x and k_y, takes the place of the Hamiltonian. The Hamiltonian character of the ray equations plays an important role in much of our analysis.

It follows from (1) and (3) that ω is constant along ray trajectories,

$$\frac{\mathrm{d}\omega}{\mathrm{d}t} = \frac{\partial\omega}{\partial x}\frac{\mathrm{d}x}{\mathrm{d}t} + \frac{\partial\omega}{\partial y}\frac{\mathrm{d}y}{\mathrm{d}t} + \frac{\partial\omega}{\partial k_x}\frac{\mathrm{d}k_x}{\mathrm{d}t} + \frac{\partial\omega}{\partial k_y}\frac{\mathrm{d}k_y}{\mathrm{d}t} = 0. \tag{4}$$

In other words, ω is a constant of the motion. The ray equations (1) are said to be integrable if a second independent constant of the motion $I(x, y, k_x, k_y)$ exists which satisfies $\mathrm{d}I/\mathrm{d}t = 0$, and whose Poisson brackets with ω vanish (see e.g. Lichtenberg & Lieberman 1983). The existence of a second constant of the motion I depends on the bathymetric variations, $h(x, y)$. If $h = h(x)$, for example, then k_y is a second constant of the motion and the ray equations (1) are integrable. For general bathymetry, however, the only constant of the motion is ω and the ray equations (1) are not integrable.

Some solutions to non-integrable Hamiltonian systems – ray trajectories in the present context – are known to exhibit chaotic behaviour, i.e. extreme sensitivity to initial conditions (see e.g. Hénon 1983; or Lichtenberg & Lieberman 1983). Thus, for general bathymetric variations, we expect that some surface gravity wave ray trajectories will exhibit chaotic motion. Throughout the remainder of this paper this idea is explored in greater detail. All of the numerical results presented are based on the bathymetric model

$$h(x, y) = h_0\left(1 + \epsilon\cos\left(\frac{2\pi x}{L}\right)\cos\left(\frac{2\pi y}{L}\right)\right), \tag{5}$$

which, in spite of its simplicity, produces chaotic ray trajectories. This bathymetric model is not corrugated, but it rather corresponds to a regular alternating pattern of bosses and dimples. More complicated (and realistic) bathymetric variations would likely produce a higher degree of ray chaos.

In the following section, the use of Poincaré sections as a tool for uncovering the presence of chaotic motion is discussed. In §3, the calculation of Lyapunov exponents is discussed. The Lyapunov exponent is a quantitative measure of how chaotic a ray trajectory is. In §4, we consider the evolution of wavecrests. These results dramatically illustrate the complexity of chaotic geometric wavefields. Some practical implications of chaotic ray trajectories are discussed in §5. Numerical considerations are discussed in Appendix A, and a proof of Liouville's theorem, as it applies to our problem, is given in Appendix B.

2. Poincaré sections

Each ray trajectory $(x(t), y(t), k_x(t), k_y(t))$ is a curve in four-dimensional phase space. But each trajectory is confined to lie on a surface of constant ω – an 'energy surface'. This constraint reduces the dimension of the region of phase space which is accessible to any ray trajectory from four to three. If a second constant of the motion exists, i.e. if the system (1) is integrable, then the dimension of the accessible region of phase space is reduced to two. If the system (1) is non-integrable then ray trajectories may either fill volumes (dimension 3) or lie on lower-dimensional surfaces (dimension 1 or 2) in the four-dimensional phase space. Such trajectories are referred to as chaotic and regular, respectively (see e.g. Hénon 1983).

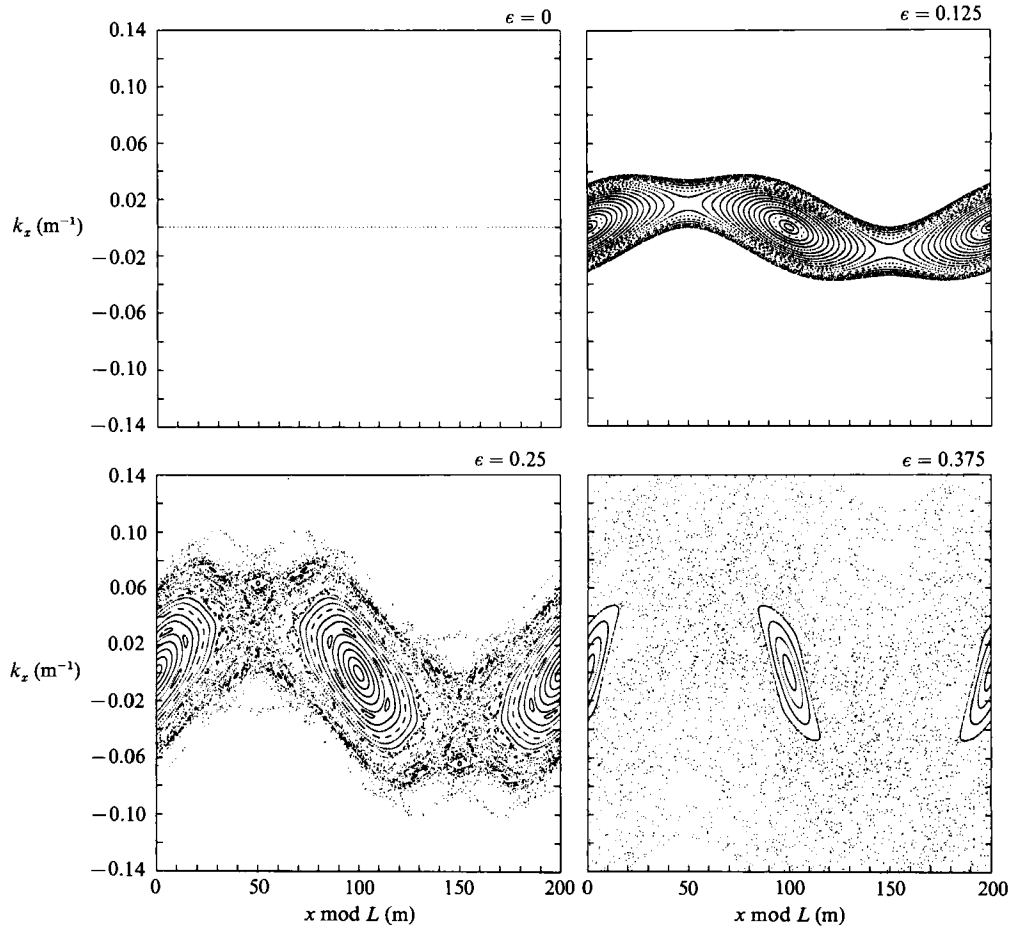

FIGURE 1. Poincaré sections for four values of ϵ, the strength of the bathymetric variability. The mean water depth h_0 and horizontal scale of the bathymetry L are fixed at 2 m and 200 m, respectively. All rays have $\omega = 2\pi/(4.80\text{ s})$. Each Poincaré section contains contributions from the 100 rays whose initial conditions are $k_x(0) = 0$, $k_y(0) = 2\pi/(20\text{ m})$, $y(0)/L = \frac{1}{4}$ and $x(0)/L = 0.01, 0.02, \ldots, 1.00$.

In order to distinguish between these two types of motion, one may view a two-dimensional slice of the full phase space. On this slice, a Poincaré section, chaotic ray trajectories fill areas while regular ones are confined to lie on smooth curves. We choose the coordinates of our Poincaré section to be the conjugate variables x and k_x. Successive intersections of a trajectory with this plane (y = constant, with the constraint $k_y > 0$) may be thought of as resulting from an implicit area-preserving mapping. These ideas are discussed in more detail by Hénon (1983).

Poincaré sections for the ray trajectories defined by (1), (2) and (5) (see also Appendix A) are shown in figures 1 and 2. Each section was constructed using 100 rays. To realize the desired reduction of dimensionality it is important that all rays in any Poincaré section lie on the same energy surface, i.e. have the same ω. From the dispersion relation (2), it is seen that this condition will be satisfied if all rays start at the same depth with the same k. For the bathymetry described by (5) a convenient choice, corresponding to points along an initially plane wave propagating in the y-direction, is $y(0) = \frac{1}{4}L$, $k_x(0) = 0$, $k_y(0) = k_0$. This choice was used in figures 1 and 2 with variable $x(0)/L$. In the ray equations (1), (2), with $h(x, y)$ given by (5), x and y

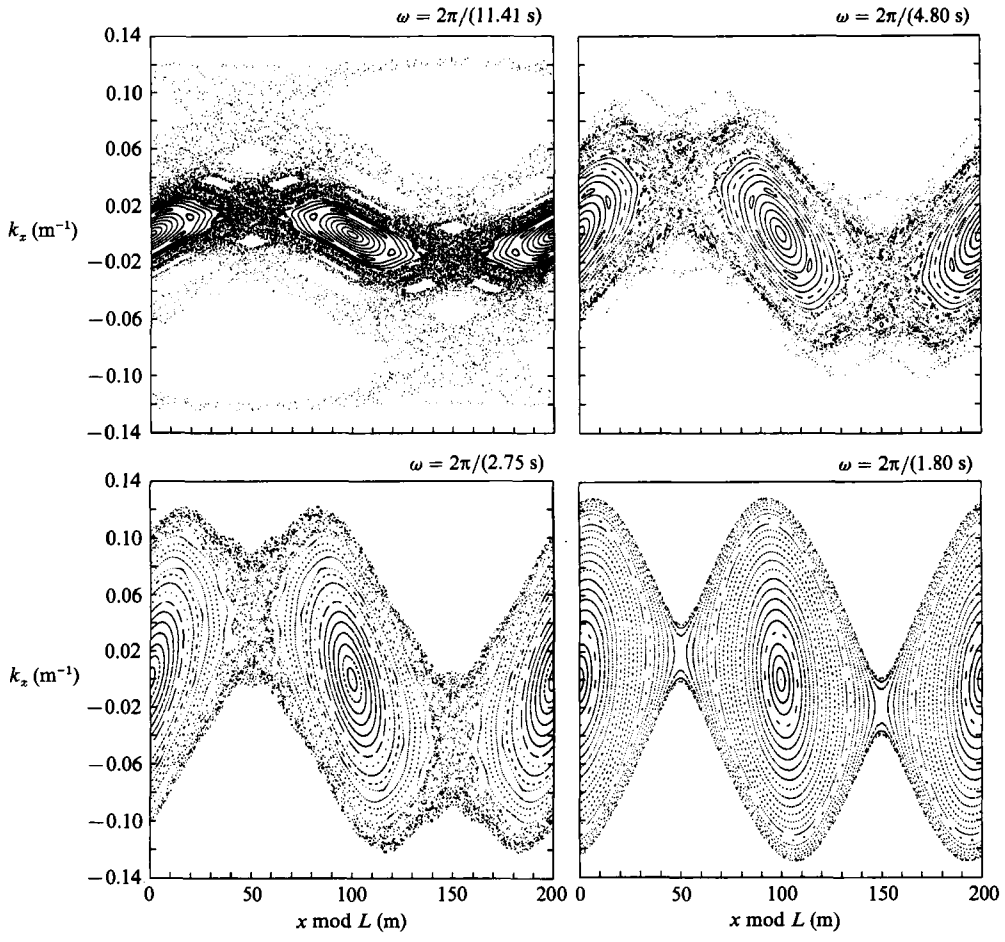

FIGURE 2. Poincaré sections for four values of frequency ω. The bathymetry is the same in all cases with $h_0 = 2$ m, $L = 200$ m and $\epsilon = 0.25$. Each Poincaré section contains contributions from the 100 rays whose initial conditions are $k_x(0) = 0$, $k_y(0) = 2\pi/\lambda_0$, $y(0)/L = \frac{1}{4}$ and $x(0)/L = -0.01, 0.02, \ldots, 1.00$. The initial wavelength $\lambda_0 = 50$ m, 20 m, 10 m and 5 m for $2\pi/\omega = 11.41$ s, 4.80 s, 2.75 s and 1.80 s, respectively.

can be defined modulo L without loss of generality. This fact was exploited in plotting x and in constructing the Poincaré sections: the intersection plane $y =$ constant was actually an infinite set of planes, $y = (n+\frac{1}{4})L$ for integer n.

The Poincaré sections shown in figure 1 show ray behaviour as a function of the strength of the bathymetric variations, ϵ. In these plots the mean water depth h_0 and the horizontal scale L of the bathymetry are fixed at 2 m and 200 m, respectively. All rays have $\omega = 2\pi/(4.80\text{ s})$. Although kh varies along ray trajectories, for the conditions considered here this product is approximately 0.63, corresponding to intermediate-depth waves. When $\epsilon = 0$ all ray trajectories are seen to be regular. This is expected because the ray equations are integrable in this case. For small but non-zero ϵ, a mixture of chaotic and regular ray trajectories is observed. The fact that some ray trajectories remain regular for sufficiently small perturbation strength ϵ is predicted theoretically: this is the content of the celebrated KAM theorem (see e.g. Lichtenberg & Lieberman 1983). As ϵ is increased, the fraction of phase space occupied by chaotic ray trajectories is seen to increase.

Figure 2 shows the frequency dependence of ray behaviour in a fixed environment ($h_0 = 2$ m, $L = 200$ m, $\epsilon = 0.25$). The frequencies selected span the intermediate-depth range. The lowest-frequency waves considered ($2\pi/\omega = 11.41$ s) correspond to values of kh near 0.25 – close to shallow water conditions. The highest-frequency waves considered ($2\pi/\omega = 1.80$ s) correspond to values of kh near 2.51 – close to deep water conditions. A higher percentage of the lower-frequency rays – which feel the bottom more strongly than the higher-frequency rays – are seen to be chaotic than is the case for the higher-frequency waves.

In Appendix A the ray equations (1), (2) for the bathymetric variations described by (5) are written in non-dimensional form, (A 2). The non-dimensional equations depend on two dimensionless parameters, ϵ and $\omega^2 h_0/g$. Each set of Poincaré sections shown in figures 1 and 2 corresponds to varying one of these parameters, holding the other fixed. By appealing to the non-dimensional equations (A 2), each Poincaré section can be rescaled to apply to a variety of choices of dimensional parameters. It must be kept in mind, however, that the ratio of the wavelength of the water wave $2\pi/k$ (which varies along a ray) to the horizontal scale of the bathymetry L should be kept small, so as not to violate the assumption of slowly varying bathymetry. For the choice of dimensional parameters used in figures 1 and 2 this ratio did not exceed approximately 0.25 and in most cases was close to 0.1.

3. Lyapunov exponents

The distinction between regular and chaotic ray trajectories is quantified by the Lyapunov exponent ν, a generalized measure of ray spreading,

$$\nu \equiv \lim_{t\to\infty} \lim_{\mathrm{d}(0)\to 0} \left[\frac{1}{t} \ln \frac{\mathrm{d}(t)}{\mathrm{d}(0)}\right]. \tag{6}$$

Here, $\mathrm{d}(t)$ is a measure of the separation in phase space between neighbouring ray trajectories. For regular trajectories $\mathrm{d}(t)$ asymptotically grows according to a power law and $\nu = 0$. All trajectories are of this type in an integrable system. This is most easily seen by expressing the solution to the ray equations (1), (2) using action-angle variables. For chaotic trajectories $\mathrm{d}(t)$ asysmptotically grows exponentially and ν is positive: ν^{-1} is the average e-folding time. There are three potential problems associated with evaluating (6) to compute ν: calculating $\mathrm{d}(t)$ and taking the limits $\mathrm{d}(0) \to 0$ and $t \to \infty$. Although any norm of the vector $(\mathrm{d}x(t), \mathrm{d}y(t), \mathrm{d}k_x(t), \mathrm{d}k_y(t))$ can be used to define $\mathrm{d}(t)$, calculating this quantity is non-trivial because $\mathrm{d}x$ and $\mathrm{d}y$ have different dimensions than $\mathrm{d}k_x$ and $\mathrm{d}k_y$. The limit $\mathrm{d}(0) \to 0$ can be investigated but only if it is done analytically. Unfortunately, the limit $t \to \infty$ is not attainable, at least using numerical methods. The procedure described below eliminates the first two of these problems but not the third.

Differentiating the ray equations (1) gives the variational equations,

$$\frac{\mathrm{d}}{\mathrm{d}t}\begin{bmatrix}\mathrm{d}x\\ \mathrm{d}y\\ \mathrm{d}k_x\\ \mathrm{d}k_y\end{bmatrix} = \begin{bmatrix}\omega_{k_x x} & \omega_{k_x y} & \omega_{k_x k_x} & \omega_{k_x k_y}\\ \omega_{k_y x} & \omega_{k_y y} & \omega_{k_y k_x} & \omega_{k_y k_y}\\ -\omega_{xx} & -\omega_{xy} & -\omega_{x k_x} & -\omega_{x k_y}\\ -\omega_{yx} & -\omega_{yy} & -\omega_{y k_x} & -\omega_{y k_y}\end{bmatrix}\begin{bmatrix}\mathrm{d}x\\ \mathrm{d}y\\ \mathrm{d}k_x\\ \mathrm{d}k_y\end{bmatrix} = \boldsymbol{\Omega}(t)\begin{bmatrix}\mathrm{d}x\\ \mathrm{d}y\\ \mathrm{d}k_x\\ \mathrm{d}k_y\end{bmatrix}. \tag{7}$$

Here $\omega_{xy} = \partial^2\omega/\partial x\,\partial y$, etc. Note that each such term in the matrix $\boldsymbol{\Omega}(t)$ depends, in general, on the ray coordinates x, y, k_x and k_y. These, in turn, are solutions to (1).

Thus, (7) and (1) constitute a system of eight coupled equations whose solution is $x(t) \ldots \mathrm{d}k_y(t)$.

Solutions to these equations – corresponding to different sets of initial conditions – can be combined to form a general set of equations relating ray spreading after time t to initial ray spreading,

$$\begin{bmatrix} \mathrm{d}x \\ \mathrm{d}y \\ \mathrm{d}k_x \\ \mathrm{d}k_y \end{bmatrix} = \begin{bmatrix} \frac{\partial x}{\partial x_0} & \frac{\partial x}{\partial y_0} & \frac{\partial x}{\partial k_{x0}} & \frac{\partial x}{\partial k_{y0}} \\ \frac{\partial y}{\partial x_0} & \frac{\partial y}{\partial y_0} & \frac{\partial y}{\partial k_{x0}} & \frac{\partial y}{\partial k_{y0}} \\ \frac{\partial k_x}{\partial x_0} & \frac{\partial k_x}{\partial y_0} & \frac{\partial k_x}{\partial k_{x0}} & \frac{\partial k_x}{\partial k_{y0}} \\ \frac{\partial k_y}{\partial x_0} & \frac{\partial k_y}{\partial y_0} & \frac{\partial k_y}{\partial k_{x0}} & \frac{\partial k_y}{\partial k_{y0}} \end{bmatrix} \begin{bmatrix} \mathrm{d}x_0 \\ \mathrm{d}y_0 \\ \mathrm{d}k_{x0} \\ \mathrm{d}k_{y0} \end{bmatrix} = \boldsymbol{J}(t) \begin{bmatrix} \mathrm{d}x_0 \\ \mathrm{d}y_0 \\ \mathrm{d}k_{x0} \\ \mathrm{d}k_{y0} \end{bmatrix}. \tag{8}$$

For a given ray trajectory – identified by its initial conditions, $x(0) \ldots k_y(0)$ – the first column of the Jacobi matrix $\boldsymbol{J}(t)$ is equal to $(\mathrm{d}x(t), \mathrm{d}y(t), \mathrm{d}k_x(t), \mathrm{d}k_y(t))^{\mathrm{T}}$ corresponding to the initial conditions $(1,0,0,0)^{\mathrm{T}}$. The second column corresponds to the initial conditions $(0,1,0,0)^{\mathrm{T}}$, etc. The determinant of the Jacobi matrix defined in this fashion is equal to unity. The constancy of $\det(\boldsymbol{J}(t))$ is a consequence of the Hamiltonian form of the ray equations. This result, a proof of which is given in Appendix B, is a statement of Liouville's theorem.

The left-hand side of (8) can be written as a linear combination of $\lambda_i u_i$ where $\boldsymbol{J}u_i = \lambda_i u_i$. Equations (8) describe the temporal evolution in phase space of an infinitesimal hypersphere (initially), centred on a given ray trajectory. As time evolves the hypersphere is deformed into an ellipsoid, but the enclosed volume remains constant. The eigenvectors u_i and eigenvalues λ_i describe, respectively, the directions of the principal axes and the rate of stretching along these axes. The product of the eigenvalues is equal to one, the determinant of the Jacobi matrix. This is a statement of phase-space volume conservation. Let λ_1 denote the eigenvalue whose modulus is greatest. Then definition (6) is equivalent to

$$\nu \equiv \lim_{t \to \infty} \frac{1}{t} \ln |\lambda_1|. \tag{9}$$

More accurately, this is the largest of four Lyapunov exponents which add to zero pairwise.

Figure 3 shows plots of $t^{-1} \ln |\lambda_1|$ for two ray trajectories, one chaotic and one regular. These results are consistent with the Poincaré section which is shown in both figures 1 and 2 corresponding to $\omega = 2\pi/(4.80\ \mathrm{s})$, $h_0 = 2$ m, $h = 200$ m and $\epsilon = 0.25$: the (chaotic) ray for which $\nu \approx (190\ \mathrm{s})^{-1}$ lies in the large chaotic sea while the (regular) ray for which $\nu \approx 0$ lies on one of curves seen in the two-island structure filling the left, centre and right of the Poincaré section.

The e-folding time ν^{-1} can be thought of as a ray 'predictability horizon'. To see this, note that under chaotic conditions $|\lambda_1|$ grows asymptotically like $10^{\nu' t}$ (here $\nu' = \nu/\ln 10$). The Lyapunov exponent expressed in base 10, ν', can be interpreted as the number of digits of information lost, on average, per unit time. If, for instance, $\nu' = 1$ min and calculations are performed on a machine with seven-digit accuracy (corresponding to 32-bit floating-point word size), then for calculated times of seven minutes or more the initial conditions of the ray will have been forgotten. In other

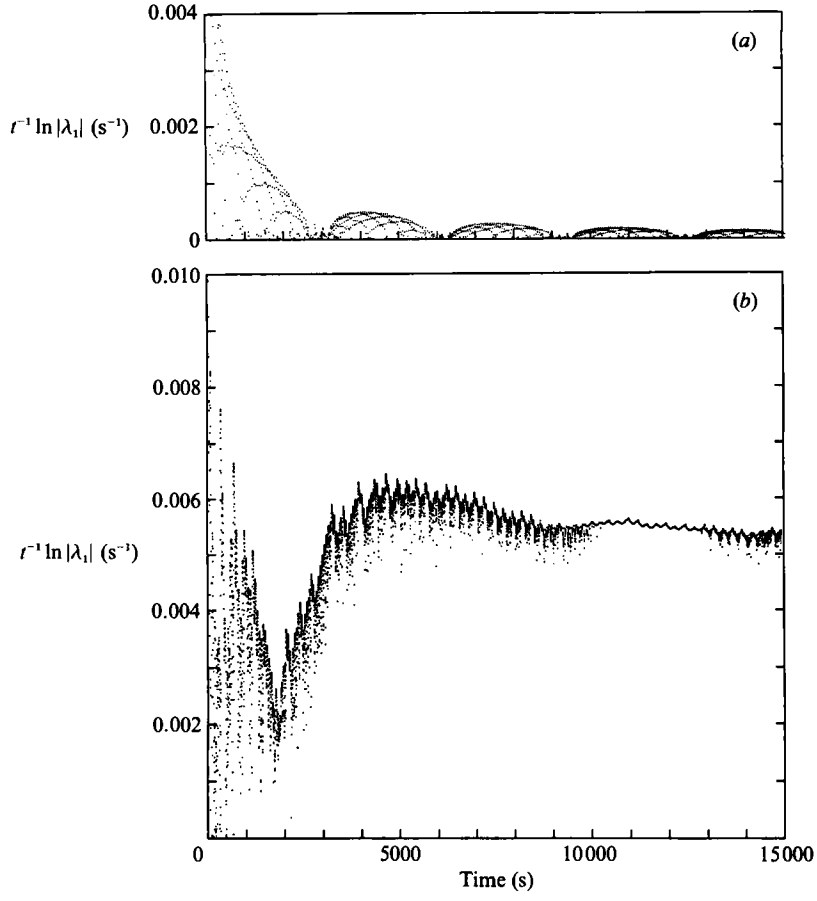

FIGURE 3. Plots of $t^{-1}\ln|\lambda_1|$ *vs.* t for two ray trajectories in the environment for which $h_0 = 2$ m, $L = 200$ m and $\epsilon = 0.25$. Both rays have initial conditions $y(0)/L = \frac{1}{4}$, $k_x(0) = 0$, $k_y(0) = 2\pi/(20\text{ m})$ and $\omega = 2\pi/(4.80\text{ s})$. (*a*) The regular ray for which $x(0)/L = 0.05$ corresponding to $\nu = 0$. (*b*) The chaotic ray for which $x(0)/L = 0.15$, corresponding to $\nu \approx (190\text{ s})^{-1}$.

words, with 32-bit floating-point arithmetic, this ray trajectory would not be computable for times in excess of somewhat less than seven minutes. Thus ν^{-1} is an order of magnitude estimate of the timescale over which a ray trajectory can be computed. The predictability timescale ν^{-1} can be converted approximately to a predictability distance scale by multiplying by a typical group speed along the ray.

4. Wavecrests

The temporal evolution of wavecrests provides insight into the difference in the complexity of chaotic and regular geometric wavefields. If most of the rays corresponding to points along such a wavecrest are chaotic with Lyapunov exponent ν, then the length of the wavecrest is expected to grow on average like $\exp(\nu t)$. If the corresponding rays are regular, on the other hand, then the length of the wavecrest will grow according to a power law. The difference is striking after only a few e-folding periods.

These ideas are illustrated in figure 4. Here, snapshots of two wavecrest segments

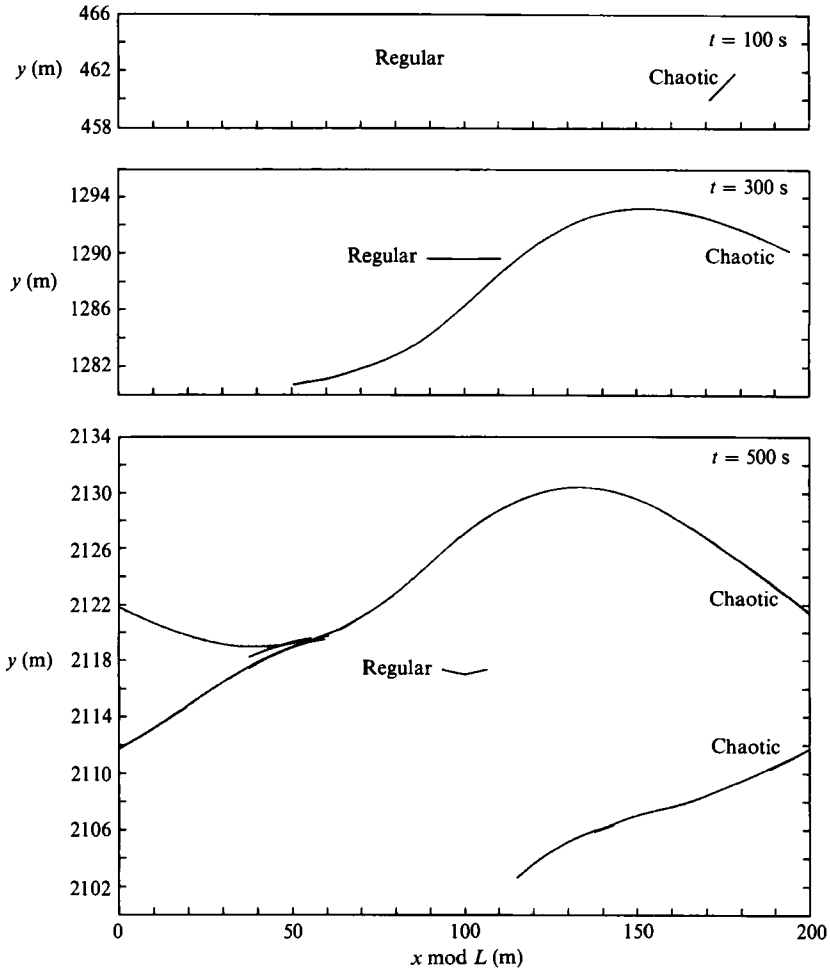

FIGURE 4. Snapshots of two wavecrest segments at three different times. Time increases from top to bottom. Both wavecrest segments were computed for the environmental conditions $h_0 = 2$ m, $L = 200$ m and $\epsilon = 0.25$. All rays along both wavecrests have initial conditions $y(0)/L = \frac{1}{4}$, $k_x(0) = 0$, $k_y(0) = 2\pi/(20\text{ m})$, corresponding to $\omega = 2\pi/(4.80\text{ s})$. The shorter wavecrest in the centre corresponds to the (mostly regular) rays for which $0.45 \leqslant x(0)/L < 0.55$. The longer wavecrest which is on the right initially corresponds to the (mostly chaotic) rays for which $0.75 \leqslant x(0)/L \leqslant 0.85$. The periodicity of x was exploited in plotting these wavecrests.

– one corresponding to mostly regular rays and one corresponding to mostly chaotic rays – are shown at three different times. These wavecrests were computed for the environmental conditions $h_0 = 2$ m, $L = 200$ m, $\epsilon = 0.25$ and frequency $\omega = 2\pi/(4.80\text{ s})$, corresponding to the Poincaré section which is shown in both figures 1 and 2: the chaotic wavefront corresponds to rays in the large chaotic sea, while the regular wavefront corresponds to rays in the two-island structure filling the left, centre and right of the Poincaré section.

Wavecrests are constructed by plotting the (x, y)-coordinates of many closely spaced (so as to approximate a continuum) ray trajectories at fixed values of phase time $t_{ph} = \int ds/c$. Here ds is arclength along a ray trajectory and $c = \omega/k$ is the phase speed. The greatest phase time shown, $t_{ph} = 500$ s, corresponds to approximately three e-folding periods of the corresponding chaotic rays ($\nu^{-1} \approx 190$ s in units of

phase time for these rays). One expects the length of the wavefront to have grown by a factor of approximately exp (3) $\approx$ 20 over this time, in rough agreement with the results shown.

The formation of cusps along the wavecrests shown in figure 4 is expected. Generically, wavecrests (surfaces of constant phase) consist of sections of certain catastrophes (see e.g. Brown & Tappert 1987). Structural stability in two dimensions, x and y, dictates that these wavecrests consist of cusps connected by smooth curves.

5. Summary and discussion

We have argued that over generic (non-separable) bathymetric variations at least some intermediate and shallow-water surface gravity wave ray trajectories are chaotic, i.e. exhibit extreme sensitivity to initial and environmental conditions. These ideas have been illustrated using a simple, analytically prescribed three-parameter (h_0, the average water depth; L, the horizontal scale of the bathymetric variations; and ϵ, the fractional change in depth associated with the bathymetric variations) bathymetric model. The surface gravity wave ray equations written in non-dimensional form were shown to depend on two dimensionless parameters, ϵ and $\omega^2 h_0/g$. It was shown that: (i) if $\omega^2 h_0/g$ is fixed, the fraction of all ray trajectories which exhibit chaotic motion increases as ϵ increases; and (ii) if ϵ is fixed, the fraction of all ray trajectories which exhibit chaotic motion decreases as $\omega^2 h_0/g$ increases. Both of these results are expected. We discussed the use of the Lyapunov exponent as a measure of how chaotic a ray trajectory is. The complexity of a chaotic geometric wavefield relative to a regular one was illustrated by considering the temporal evolution of segments of wavecrests.

It is natural to ask whether the effects we have described, such as the exponential stretching of segments of wavecrests, occur in nature. The answer is probably not. To understand why, note that the ray equations (1), (2) correspond to the geometric or classical limit of the mild-slope equation (see e.g. Mei 1983) – a linear wave equation for the surface displacement $\zeta(x, y, t)$. Because this equation is linear its solutions cannot be chaotic in the strict sense, namely, exponential sensitivity in the limit $t \to \infty$. Physically, the absence of chaos in solutions to the mild-slope equation can be understood by noting that effects of wave diffraction, which are not present in our analysis, will serve to smooth out small details of the geometric wavefields we have considered. These effects are most important at lower frequencies. But it is the lower-frequency waves which are most sensitive to bathymetric variations and hence the most likely to be chaotic. Thus, loosely speaking, the importance of diffractive effects grows as the likelihood of chaotic ray trajectories increases. In addition to diffractive effects, which are present in the solutions of the linear (small-amplitude) equations of motion, nonlinear finite-amplitude effects will be present in nature. These may also serve to overcome behaviour associated with chaotic ray trajectories by, for example, causing closely spaced segments of a wavecrest to coalesce. On the other hand, finite-amplitude instabilities (e.g. Benjamin 1967) may cause wavecrests to break up into chaotic short-crested waves. Chaotic solutions of the finite-amplitude wave equations will differ from the ray chaos that we have investigated.

Even if the effects associated with chaotic surface gravity wave ray trajectories that we have described are not observable in nature, this study still has important practical implications in the field of coastal hydrodynamics. The Shore Protection Manual (CERC 1977) recommends the use of computer ray tracing models (see e.g. Hardy 1968) for the construction of 'refraction diagrams' to predict the effects of

refraction by bathymetry. This study addresses and quantifies the limitations of making such predictions under chaotic conditions, i.e., when variables cannot be separated. Under such conditions, predictions using ray theory must be limited to times and distances within some finite 'predictability horizon' (Lighthill 1986). At greater times, ray trajectories will have effectively forgotten their initial conditions and are of little value – at least for making deterministic predictions. Under such conditions, wavefield predictions must be based on the numerical solution to a wave equation such as the mild-slope equation or some finite-amplitude extension thereof. For the problem we have investigated (recall that $\nu^{-1} \approx 190$ s and $\omega = 2\pi/(4.80\text{ s})$ for a ray which was used to produce figure 3) loss of predictability occurs after a few hundred wave periods. This is approximately the outer limit of the domain over which the neglect of finite-amplitude effects is expected to be valid. Thus, ray chaos provides an additional reason not to use the ray approximation beyond generally accepted limits.

In addition to this computational issue, our results suggest that the distinction between separable and non-separable linear wave propagation problems is deeper than noting that we are able to express the solution to the former but not the latter class of problems in terms of elementary functions and integrals: in the geometric limit, at least, the behaviour of the solution to these two types of problem is fundamentally different.

We are grateful to Drs B. Le Mehaute, J. Willemsen and A. Griffa for the benefit of our discussions on water waves and chaos. This work was supported by the Office of Naval Research and the National Science Foundation.

Appendix A. Numerical considerations

All of the numerical results reported in this paper require the integration of systems of coupled nonlinear ordinary differential equations. These are either the ray equations (1), (2) or the coupled ray – variational equations (1), (2), (7). In the following, some simple considerations relating to this task are discussed. First, we point out that the constancy of ω along ray trajectories (4) can be used to both simplify and improve the accuracy of these calculations. Then we show that for bathymetric variations described by (5) the non-dimensionalized ray equations depend on two dimensionless parameters. Finally, checks on the accuracy of our calculations are discussed.

The ray (1) and variational equations (7) involve, respectively, first and second partial derivatives of ω (2) with respect to x, y, k_x and k_y. These are somewhat messy expressions which involve the hyperbolic functions $\tanh kh$ and $\operatorname{sech}^2 kh$. These functions need not be evaluated, however. It follows from the dispersion relation (2) that $\tanh kh = \omega^2/(gk)$ and $\operatorname{sech}^2 kh = 1-\omega^4/(g^2k^2)$. The latter expressions are particularly simple to evaluate because, from (4), $\omega(t) = \omega(0)$, i.e. ω is constant along any ray trajectory. Thus, making these substitutions simultaneously reduces the number of required floating-point operations (significantly) and improves the accuracy of the results – because potential errors associated with the evaluation of $h(x(t), y(t))$, $\tanh kh$ and $\operatorname{sech}^2 kh$ have been eliminated. With these comments in mind, these partial derivatives are numerically evaluated in the following form:

$$\frac{\partial\omega}{\partial x_i} = \frac{1}{2\omega g}(g^2k^2-\omega^4)\frac{\partial h}{\partial x_i}, \quad \frac{\partial\omega}{\partial k_i} = \frac{\omega k_i}{2k^2}\left[1+\frac{h}{\omega^2 g}(g^2k^2-\omega^4)\right], \qquad (A\,1a, b)$$

$$\frac{\partial^2\omega}{\partial x_i\,\partial x_j} = \frac{1}{2\omega g}(g^2k^2-\omega^4)\left[\frac{\partial^2 h}{\partial x_i\,\partial x_j} - \frac{1}{2\omega^2 g}(3\omega^4+g^2k^2)\left(\frac{\partial h}{\partial x_i}\right)\left(\frac{\partial h}{\partial x_j}\right)\right], \tag{A 1c}$$

$$\frac{\partial^2\omega}{\partial k_i\,\partial k_j} = \frac{\omega}{2k^2}\left[1+\frac{h}{\omega^2 g}(g^2k^2-\omega^4)\right]\delta(k_i,k_j) - \frac{\omega k_i k_j}{k^4}\left[\tfrac{3}{4}+\frac{h^2}{g^2}(g^2k^2-\omega^4)+\tfrac{1}{4}\left(\frac{h}{\omega^2 g}\right)^2(g^2k^2-\omega^4)^2\right], \tag{A 1d}$$

$$\frac{\partial^2\omega}{\partial x_i\,\partial k_j} = \frac{k_j}{4\omega g k^2}(g^2k^2-\omega^4)\left[3-\frac{h}{\omega^2 g}(3\omega^4+g^2k^2)\right]\left(\frac{\partial h}{\partial x_i}\right). \tag{A 1e}$$

Here $x_i = x$ or y, $k_i = k_x$ or k_y and $\delta(k_i, k_j) = 1$ if $k_i = k_j$ and 0 if $k_i \neq k_j$.

For the bathymetric variations described by (5), it is instructive to write the ray equations in non-dimensional form. For numerical purposes this is convenient but not necessary. In terms of the dimensionless variables $t^0 = h_0\,\omega t/L$, $x^0 = x/L$, $y^0 = y/L$, $k_x^0 = k_x h_0$, $k_y^0 = k_y h_0$ and $k^0 = k h_0$ these equations are

$$\frac{\mathrm{d}x^0}{\mathrm{d}t^0} = \frac{k_x^0}{2(k^0)^2}\left\{1+\frac{\omega^2 h_0}{g}\left[\left(\frac{g}{\omega^2 h^0}\right)^2(k^0)^2-1\right][1+\epsilon\cos(2\pi x^0)\cos(2\pi y^0)]\right\}, \tag{A 2a}$$

$$\frac{\mathrm{d}y^0}{\mathrm{d}t^0} = \frac{k_y^0}{2(k^0)^2}\left\{1+\frac{\omega^2 h_0}{g}\left[\left(\frac{g}{\omega^2 h_0}\right)^2(k^0)^2-1\right][1+\epsilon\cos(2\pi x^0)\cos(2\pi y^0)]\right\}, \tag{A 2b}$$

$$\frac{\mathrm{d}k_x^0}{\mathrm{d}t^0} = \pi\epsilon\left(\frac{\omega^2 h_0}{g}\right)\left[\left(\frac{g}{\omega^2 h_0}\right)^2(k^0)^2-1\right]\sin(2\pi x^0)\cos(2\pi y^0), \tag{A 2c}$$

$$\frac{\mathrm{d}k_y^0}{\mathrm{d}t^0} = \pi\epsilon\left(\frac{\omega^2 h_0}{g}\right)\left[\left(\frac{g}{\omega^2 h_0}\right)^2(k^0)^2-1\right]\cos(2\pi x^0)\sin(2\pi y^0). \tag{A 2d}$$

These equations are seen to depend on two dimensionless parameters – ϵ and $\omega^2 h_0/g$ – which govern the stochasticity of the ray trajectories.

The non-dimensional form of the ray equations illustrates an important point. Chaotic motion is often defined as unpredictable motion of a deterministic nonlinear system owing to extreme sensitivity to initial conditions. But the non-dimensional variables depend on environmental parameters, which, when perturbed, cause a perturbation to the non-dimensional initial conditions. Thus, extreme sensitivity applies to both initial and environmental conditions.

All numerical calculations were performed using a fourth-order Runge–Kutta algorithm with a fixed step size of $\Delta t^0 = 0.005$ or smaller. Both the ray equations and the coupled ray–variational equations were integrated in dimensional form. Double-precision arithmetic, i.e. 64-bit floating-point wordsize, was used for all calculations. To check the accuracy of the calculations, the constancy of ω and phase-space volume ($\det \boldsymbol{J} = 1$ – for the Lyapunov exponent calculation) along ray trajectories were checked at regular intervals. In no case did the fractional errors, $(\omega(t)-\omega(0))/\omega(0)$ and $\det \boldsymbol{J}(t)-1$, exceed 1.0×10^{-8} and 1.0×10^{-6}, respectively.

Appendix B. A proof of Liouville's theorem

In the following, a direct proof of the result $\det(\boldsymbol{J}(t)) = 1$, where $\boldsymbol{J}(t)$ is the Jacobi matrix defined in (8), is given. This is a statement of Liouville's thoerem. This result, which follows from the Hamiltonian form of the ray equations (1), (2), is important

theoretically and provides a means of checking the accuracy of the numerical integration of the coupled ray–variational equations (1), (2), (7) as discussed in Appendix A.

Let $\boldsymbol{\delta}(t)$ denote the column vector $(\mathrm{d}x(t), \mathrm{d}y(t), \mathrm{d}k_x(t), \mathrm{d}k_y(t))^{\mathrm{T}}$. Then the variational equations (7) can be written

$$\frac{\mathrm{d}}{\mathrm{d}t}\boldsymbol{\delta}(t) = \boldsymbol{\Omega}(t)\,\boldsymbol{\delta}(t). \tag{B 1}$$

The solution to this equation is given by equation (8),

$$\boldsymbol{\delta}(t) = \boldsymbol{J}(t)\,\boldsymbol{\delta}(0). \tag{B 2}$$

The Jacobi matrix $\boldsymbol{J}(t)$ can be expressed formally as

$$\boldsymbol{J}(t) = \mathrm{T}\exp\left(\int_0^t \boldsymbol{\Omega}(t')\,\mathrm{d}t'\right) \tag{B 3}$$

where T is Dyson's time ordering operator. The determinant of $\boldsymbol{J}$ is related to the trace of $\boldsymbol{\Omega}$,

$$\det \boldsymbol{J}(t) = \mathrm{T}\exp\left(\int_0^t \mathrm{tr}\,[\boldsymbol{\Omega}(t')]\,\mathrm{d}t'\right). \tag{B 4}$$

By inspection of the variational equations (7),

$$\mathrm{tr}\,[\boldsymbol{\Omega}(t)] = 0. \tag{B 5}$$

It follows that

$$\det \boldsymbol{J}(t) = 1, \tag{B 6}$$

which completes the proof.

REFERENCES

BENJAMIN, T. B. 1967 Instability of periodic wavetrains in nonlinear dispersive systems. *Proc. R. Soc. Lond.* A **299**, 59–75.

BROWN, M. G. & TAPPERT, F. D. 1987 Catastrophe theory, caustics, and travel time diagrams in seismology. *Geophys. J. R. Astr. Soc.* **88**, 217–229.

CERC (Coastal Engineering Research Center) 1977 Wave refraction. In *Shore Protection Manual*, 3rd Edn., Vol. I, Sect. 2.3. US Government Printing Office, Washington, D.C.

HARDY, J. R. 1968 Some grid and projection problems in the numerical calculation of wave refraction. *J. Geophys. Res.* **73**, 7083–7087.

HÉNON, M. 1983 Numerical exploration of Hamiltonian systems. In *Chaotic Behavior of Deterministic Systems: Les Houches Lectures 36* (ed. G. Iooss, R. G. H. Helleman & R. Stora), pp. 171–271. North-Holland.

LANDAU, L. D. & LIFSHITZ, E. M. 1959 *Fluid Mechanics*, pp. 256–259. Pergamon.

LICHTENBERG, A. J. & LIEBERMAN, M. A. 1983 *Regular and Stochastic Motion*. Springer.

LIGHTHILL, J. 1986 The recently recognized failure of predictability in Newtonian dynamics. *Proc. R. Soc. Lond.* A **407**, 35–50.

MEI, C. C. 1983 *The Applied Dynamics of Ocean Surface Waves*. Wiley Interscience.

WHITHAM, G. B. 1974 *Linear and Nonlinear Waves*. Wiley Interscience.